Research Article

Steady-State Flow Characteristics and End Clearance Optimization of Internal Gear Grease Pump

Xinjian Li ⓘ**, Lingfeng Tang, and Ming Qian**

School of Mechanical Engineering, Anhui Polytechnic University, Wuhu, Anhui 241000, China

Correspondence should be addressed to Xinjian Li; 2190130115@stu.ahpu.edu.cn

The internal gear grease pump is a mechanical device used for transfer of high viscosity fluid. The existing clearance between the end faces of the internal or external gear and the floating side plate might cause pump leakage during operation. In order to obtain the optimal end clearance of the internal gear grease pump, the rheological features of the lubricating lithium-based grease for various temperatures are explored via rotating rheometer. Shear force and apparent viscosity are chosen as monitored experimental parameters. The experimental data is fitted to obtain grease rheological features at various temperatures. The end clearance flow field model and the leakage model are established. Fluent software is employed for solving the flow field model and exploring the effect of temperature, end clearance, and speed on grease leakage. Superior grease flow performance is observed with an increase in temperature, which makes it to easier for the grease to leak from the end clearance. With an increase in the end clearance and the working pressure of the pump, an increase in leakage is also observed. Furthermore, it is found that rotational speed also affects the pump leakage. The leakage mechanism is obtained by combining the rheological features of the grease at the end clearance. The mathematical model method is utilized to solve for the optimal value of the end clearance.

1. Introduction

The compact structure and small flow pulsation of the internal gear pump contribute to its wide usage in industrial fields that require high precision, energy saving, high environmental noise, and high reliability. Similar to other types of pumps, internal gear pump leakage, as well as the end leakage, is often problematic. The end clearance of the internal gear pump is formed by the friction pair between the end faces of internal and external gears and the floating side plate. Thus, successful prevention of end leakage can significantly improve the volumetric efficiency of the pump.

Schweiger et al. [1] established the flow field model of the end clearance and radial leakage of the internal gear pump. The authors employed numerical simulations to explore the effect of temperature on the end clearance and radial clearance leakage. The leakage will cause the power loss of the internal gear pump. Guo [2] used the CFD method to numerically simulate the pressure field and the velocity field and analyzed the effects of extrusion power loss, pressure

and viscous power loss, rotation speed, and tooth width on flow field characteristics. Zeng [3] established the geometric relationship during the meshing process, and the unloading area expression was obtained by using the geometric pattern expansion method with the variable f as the independent variable. A few scholars [4–7] also applied different algorithms to optimize the parameters of internal gear pump. However, when grease is employed as the pump medium, which is a non-Newtonian fluid and has unique rheological features, it is necessary to investigate its physical properties. Bingham [8] studied the plastic fluids and found that when the stress exceeded the yield strength of the material, it maintained a proportional relationship with strain. This observation is now called the Bingham model. Herschel and Bulkley [9] utilized three parameters to establish a theoretical model of the relationship between grease shear stress and shear rate. This model was named the H-B model. Radulescu [10] and Radulescu employed the Bingham model to investigate the application of calcium-based and lithium-based lubricating grease. The authors found that the H-B

model provided better correlation of rheological features of the two greases with the experimental data. Many studies have been conducted on mechanisms of grease change, structure, and application of laws in engineering practice. Mohamed [11] used high-resolution transmission electron microscope (HRTEM) and scanning electron microscope (SEM) to study the microstructure of CNTs and lithium lipids. Hamrock and Dawson [12] found that when the grease is subjected to higher shear stress, the viscosity of the grease maintains a linear change within a certain range. When the influence of grease fiber content on the rheological features ranged from 2% to 16%, it was found that the soap fiber content negatively correlates with grease rheological index, while positive correlation is observed with grease yield stress [13]. Wang et al. discovered BN nanoparticles can not only produce lubricating film to protect friction pairs, but also their layered structure is easy to cause sliding of the friction pairs under the action of friction [14]. Simultaneously, the pipeline or transportation equipment grease temperature increase caused by friction also affects the internal structure of the grease. The variation of physical entanglement caused by short heat treatment changed the tribological properties of the lithium-based lubricating grease [15]. On the other hand, many domestic researchers have not specifically studied the influence of grease as medium on pump performance.

In this paper, a rotating rheometer is employed to explore the rheological features of lithium-based lubricating grease at the end clearance with consideration of different temperatures. Fluent software is used to simulate the flow field of the model and to explore the effects of temperature, end clearance, and rotational speed on the end clearance leakage. Based on the basic equations of fluid dynamics, as well as the grease rheological model, the end clearance leakage model of the internal gear grease pump is developed. The mathematical model method is employed to optimize the end clearance and investigate the leakage mechanism.

2. Research on the Rheological Features of Grease

In order to study the pump leakage mechanism at the end clearance, it is necessary to study the rheological features of the grease and explore the influence of the grease characteristics on the end clearance leakage itself. The NLGI 1 lubricating grease is usually used in internal gear pumps [16]. Performance parameters of several lubricating greases are shown in Table 1.

Based on data provided in Table 1, it can be concluded that the lithium-based lubricating grease, calcium-based lubricating grease, and complex calcium-based lubricating grease have higher penetration, but according to the temperature set by the experiment, calcium-based lubricating grease cannot meet the temperature requirements, and the water resistance of complex calcium-based lubricating grease is not suitable for the experimental environment. Therefore, lithium-based lubricating grease is selected as the experimental material.

2.1. Test of Rheological Features of Grease.
The NLGI 1 lithium-based lubricating grease is selected as the experimental material, while the rotating rheometer (MCR302) is employed for the test (Figure 1). The H-B model is used to investigate the viscosity and grease shear rate stress variation at different temperatures and shear rates. Experimental temperature was in the range of 25°C to 85°C, while the shear rates controlled by the rotating rheometer were within the range of $0.01 \, s^{-1}$ to $100 \, s^{-1}$.

2.2. Grease Flow Characteristics Analysis.
According to Figure 2(a), the shear stress of NLGI 1 lithium-based lubricating grease increases with the shear rate. Lubricating grease is a structural colloidal dispersion system. Its saponified structure causes the grease to have a certain structural strength. As a result, it demonstrates solid non-flowing characteristics in the early stage and mainly undergoes elastic deformation. After the early stage, the grease starts to show viscous flow. The shear stress curve plotted against the shear rate conforms to the power law [17]. On the other hand, Figure 2(b) demonstrates that the apparent viscosity of the grease gradually decreases with an increase in the shear rate. By comparing the curves on Figures 2(a) and 2(b), it can be observed that viscosity decreases with an increase in temperature. However, unstable regions in the flow curve are present due to the wall slip effect, which influences the grease flow [18].

In order to discuss the changes of apparent viscosity of grease more intuitively, a set of grease viscosity data can be selected, and logarithmic coordinates can be replaced with the ordinary ones. The result is shown in Figure 3.

Based on the experimentally obtained grease flow curves, it can be observed that the H-B model can accurately characterize the viscous flow characteristics of the grease [9]. Therefore, the H-B model is employed for data fitting to obtain the rheological parameters (τ_0, k, n) of NLGI 1 lithium-based lubricating grease at various temperatures. The specific values are shown in Table 1.

Based on the data provided in Table 2, it can be concluded that the yield strength, consistency coefficient, and shear thinning index of the grease decrease with the increase in temperature. This shows that an increase in temperature enhances the grease flow performance and further increases the leakage of the end clearance.

2.3. Change Mechanism of Grease Rheological Features.
Figure 4 shows the micromorphology of NLGI 1 lithium-based lubricating grease observed under the scanning electron microscope. It can be observed that the grease fibers are entangled into a network structure. This structure itself hinders the flow of grease, but it can enhance it when accompanied by continuous shearing force and temperature increase. Considering that the grease is affected by the shear stress and frictional heat [15, 19], it is necessary to fully consider the influence of the rheological features of the grease leakage in the end clearance zone.

TABLE 1: Performance parameters of various lubricating greases.

Type of greases	Temperature (°C)	Penetration (0.1 mm)	Drop point (°C)	Water resistance
Lithium-based lubricating grease	−20~120	325	178	Better
Calcium-based lubricating grease	−10~60	322	80	Better
Graphite calcium-based lubricating grease	−10~600	265	80	General
Complex calcium-based lubricating grease	−10~150	310	180	Worse
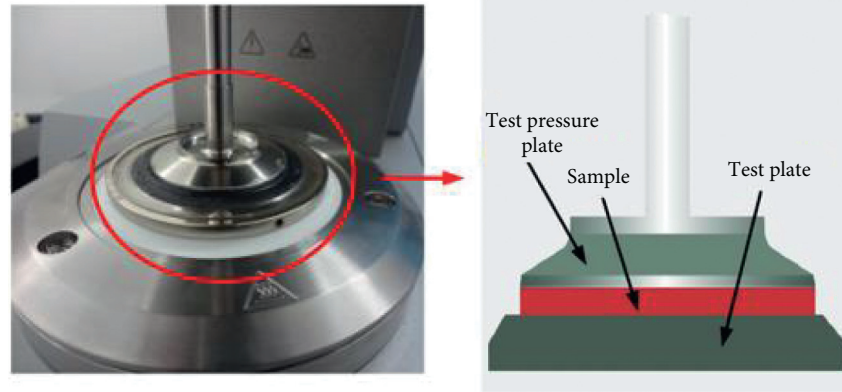
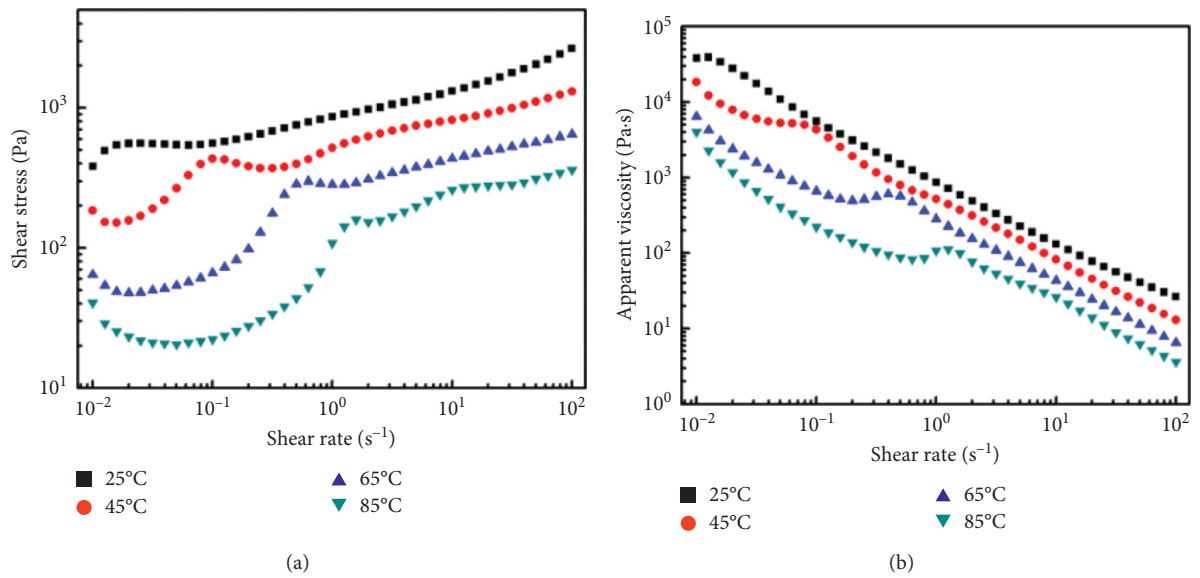FIGURE 1: MCR 302 rotating rheometer and test module.

FIGURE 2: Variation of shear stress and apparent viscosity of the grease with shear rate at different temperatures for (a) curve of the shear stress with the shear rate and (b) curve of the apparent viscosity with the shear rate.

Figure 5 depicts the frequency sweep curve with frequency (tan δ) of the storage modulus (G') and loss modulus (G'') of NLGI 1 lithium-based lubricating grease at various temperatures. It can be observed that, in the entire frequency sweep area, the storage modulus of the grease at each temperature is greater than the loss modulus. Furthermore, the higher the temperature, the greater the values of the storage modulus and loss modulus. Therefore, the entanglement of NLGI 1 lithium-based grease can be characterized by the platform modulus (G_N^0) [12]. The platform modulus of the lubricating grease can be obtained by extrapolating from the experimental data of the grease frequency sweep, which can be expressed by the following formula:

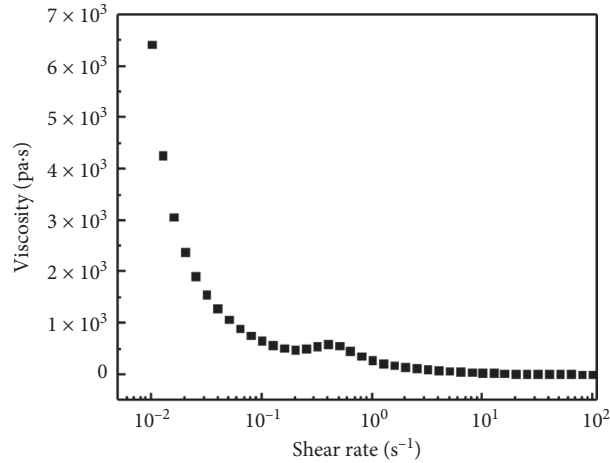$$G_N^0 = [G']_{\tan \delta \longrightarrow \text{minimum}}. \tag{1}$$

FIGURE 3: Curve of the apparent viscosity of NLGI 1 lithium-based lubricating grease as a function of the shear rate.

TABLE 2: Rheological parameters of NLGI 1 lithium-based lubricating grease at various temperatures.

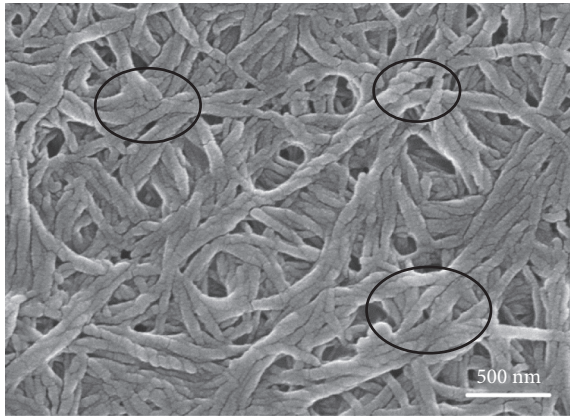| Temperature (°C)	Yield strength (Pa)	Consistency coefficient (Pa S^n)	Shear thinning index
25	542	286.40	0.43
45	350	136.51	0.45
65	283	43.25	0.48
85	132	27.44	0.49

FIGURE 4: Micromorphology of NLGI 1 lithium-based lubricating grease.

3. Numerical Simulation of the Flow Field at the End Clearance of the Internal Gear Grease Pump

In order to explore the leakage mechanism of the end clearance with greater accuracy, the clearance flow field model is established, the ICEM CFD software is employed to divide the mesh, and Fluent software is used to solve the model.

3.1. Meshing the Flow Field Model. The end clearance leakage of internal gear pump conforms to the double disc leakage model. The leakage area of the external gear is defined as the area from the root circle of the external gear to the gear shaft. The leakage area of the internal gear is defined as the area from the root circle of the internal gear to the outer circle of the gear. It should be noted that the leakage area is not a complete disc, but rather a disc fraction falling between the angles of the internal and external gear leakage of 131.718° and 158.09°, respectively. The clearance values are taken as 0.03 mm, 0.04 mm, 0.05 mm, and 0.06 mm. Figure 6 depicts the flow field model.

The ICEM CFD preprocessing software is utilized to mesh the flow field model. In Figure 6, it can be observed that the grid has a certain periodicity. Therefore, the flow field model can be divided into periodic meshes [19], which can simplify the flow field model for the purpose of obtaining higher-quality grid. Three boundary layers are added to the grid, which is shown in Figure 7.

3.2. Boundary Conditions. During the operating process of the internal gear pump, the leakage of the end clearance occurs mainly due to the flow resulting from pressure difference. The pressure inlet of the pump is rated at 25 MPa, while the pressure outlet is rated at 0.1 MPa. The specific boundary conditions are presented in Table 3.

3.3. Analysis of Simulation Results. Temperature simulation parameters are selected according to Table 1. The simulation is carried out via *Fluent* software with the lubricating grease rheological parameters at 25°C, 45°C, 65°C, and 85°C. The simulation results are exported by Tecplot 360 EX 2015 R1 and its own postprocessing software, as shown in Figure 8:

According to Figure 8, the grease traverses in a laminar flow and is symmetrically distributed within the clearance. With an increase in pump temperature, the clearance grease
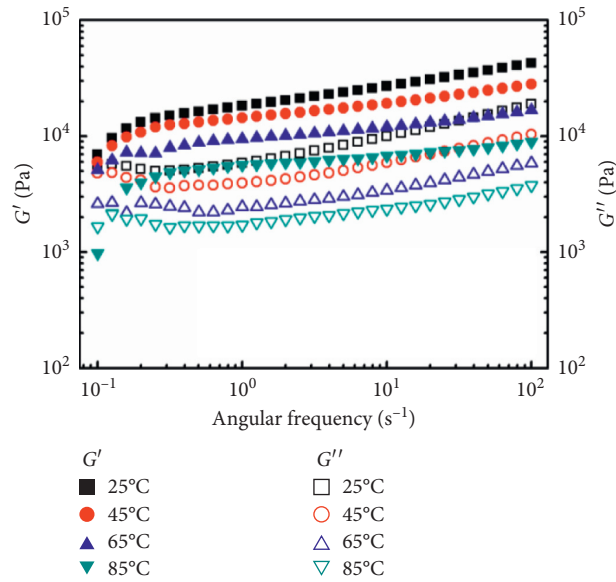
Figure 5: Frequency sweep curve of NLGI 1 lithium-based lubricating grease at different temperatures.
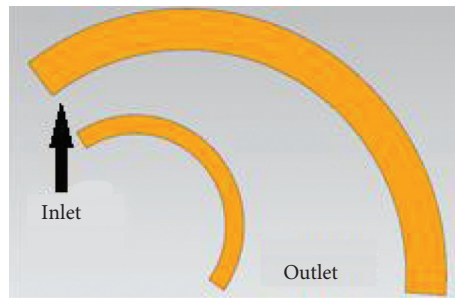

Figure 6: Flow field model of end clearance of internal gear pump.
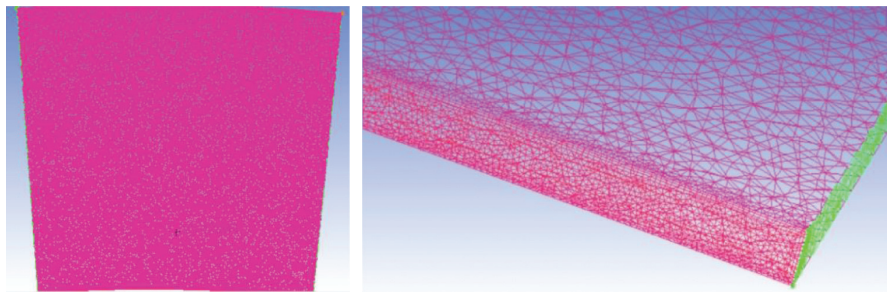

Figure 7: End clearance flow field grid.

Table 3: Boundary conditions of numerical simulation.

Calculation conditions	Parameter
Density	$900 \, \text{kg/m}^3$
Inlet	25 MPa
Outlet	0.1 MPa
Upwind	Second-order upwind
Method	Simple

flow rate increases significantly. In combination with Figure 9, it can be observed that the grease flow increases under pressure after overcoming its yield strength from the inlet to the outlet. Due to the high shear rate at the wall, the grease reaches its yield strength and gradually forms a flow core. Then, the grease forms a plug flow in the clearance. With an increase in the shear rate, the size of the flow core decreases. Finally, the flow becomes laminar. It can be concluded from

25°C

Inlet section

Outlet section

(a)

45°C

Inlet section

Outlet section

(b)

65°C
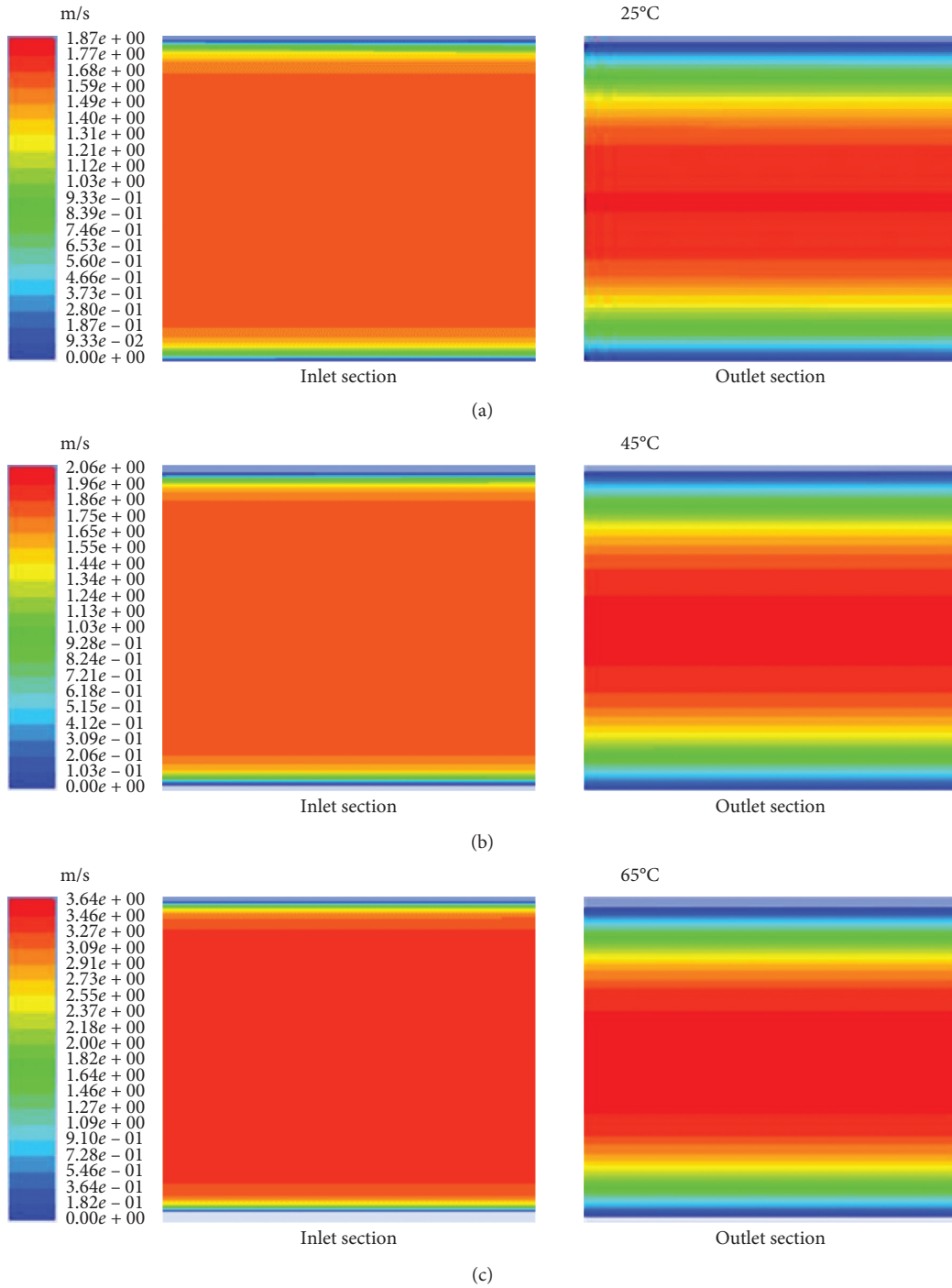
Inlet section

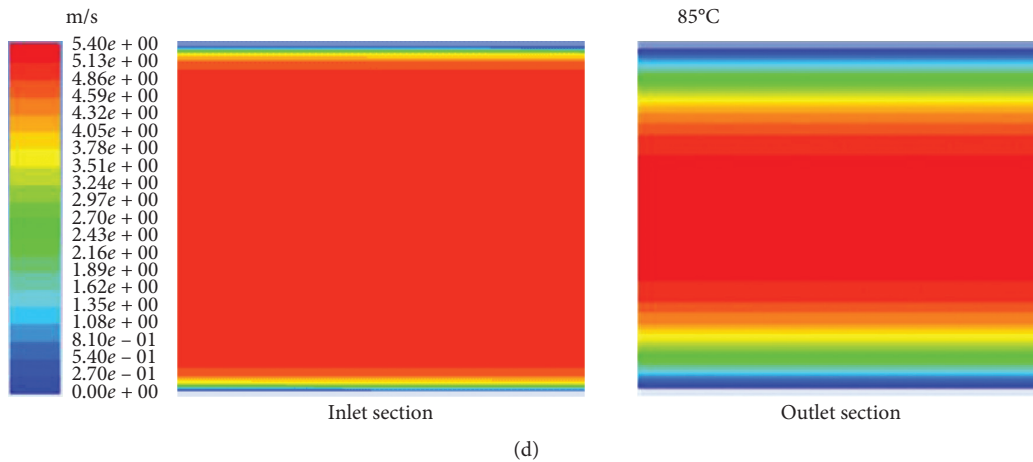Outlet section

(c)

FIGURE 8: Continued.

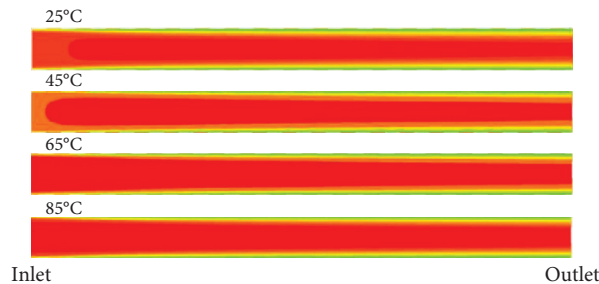Figure 8: Vectors of velocity at inlet and outlet section at 25°C–85°C.

Figure 9: Vectors of velocity at radial section at 25°C–85°C range.

Figure 9 that, at 25°C, a sudden pressure drop at the inlet is observed, which then uniformly changes, as illustrated in Figure 10. At 65°C and 85°C, the pressure changes more evenly from the inlet to the outlet. Generally speaking, the lower the temperature is, the more the pressure will be consumed during the inlet phase.

Based on the aforementioned results, it can be concluded that, with an increase in temperature, grease and end clearance leakage flow characteristics are both increased. However, this does not necessarily mean that lower temperatures are preferable. Although the leakage is reduced in the low temperature regions, the yield strength and viscosity of the grease are increased. This results in an upsurge in the required starting torque, as well as generated fluid friction. After comprehensive consideration, 65°C is chosen as the optimal pumping temperature.

Numerical clearance effect simulation results are shown in Figures 11 and 12. The clearances are taken as 0.04 mm, 0.05 mm, and 0.06 mm, while a temperature of 65°C is utilized for numerical simulation.

It can be clearly seen from Figure 11 that the clearance value increase causes a surge in the end clearance grease flow rate. This suggests that the flow at the inlet and the outlet of the clearance will occupy more areas. When the pressure gradient remains unaltered, the shear rate of the grease at the wall increases with an increase in the clearance value. The apparent viscosity of the grease decreases with an increase of the shear rate; that is, the grease will flow more easily at the

clearance while gradually increasing its flow rate [19]. Figure 12 also verifies this point. With an increase in the clearance value, the leakage section will also grow. Due to the combined influence of the two, the end clearance leakage will increase significantly.

In order to explore the effect of rotation speed on the leakage at the end clearance, the rotation speeds of $1000 \, min^{-1}$, $1500 \, min^{-1}$, and $2000 \, min^{-1}$ are employed, while the temperature is kept at 65°C. The results are shown in Figure 13.

From Figure 13, it can be seen that the grease flow is still laminar in the clearance region. However, the velocity distribution along the clearance direction is no longer symmetrical. This is caused by the plate drag effect formed by the rotation of the gear side, which increases the flow speed of the grease on the gear side, making it greater than that of the floating side plate, whose effect can be neglected.

From Figures 14(a)–14(c) and Figure 15, it can be seen that the end clearance leakage flow gradually increases in the internal gear leakage area with the rotational speed, and the pressure difference between two adjacent teeth of pressure transition zone becomes larger with the increase of the pump rotary speed [20]. In the external gear leakage area, with an increase in the rotational speed, the clearance flow leakage gradually decreases. This phenomenon occurs because the direction of the centrifugal force generated by the gear rotation is opposite to the flow direction generated by the grease pressure. Therefore, the higher the rotational speed is,
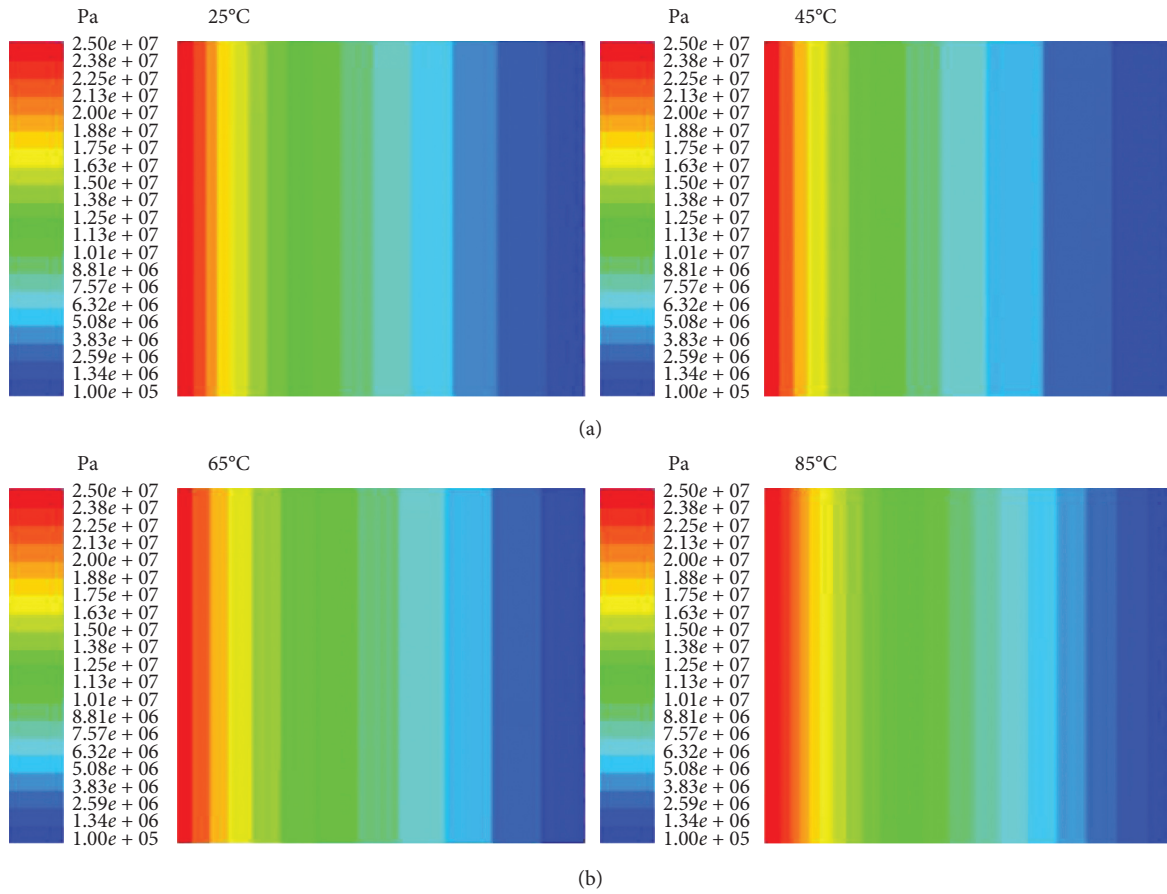
(a)

(b)

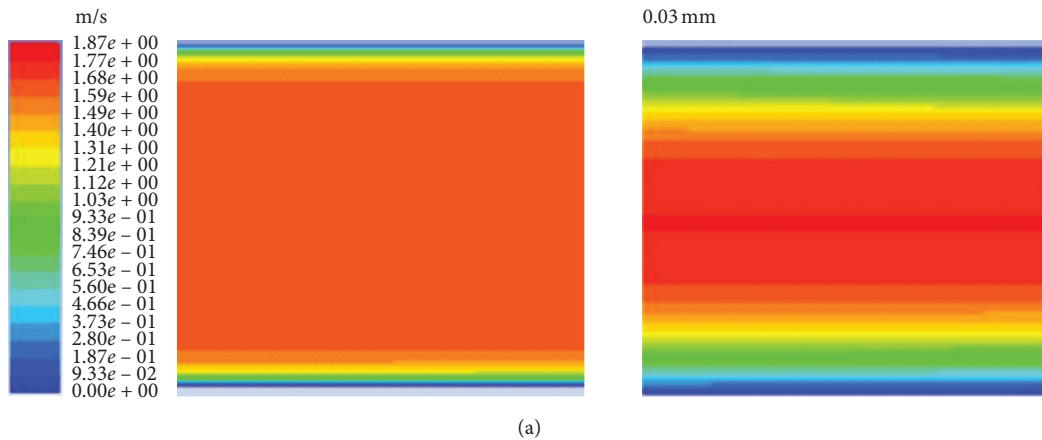FIGURE 10: Vectors of pressure from inlet to outlet at 25°C–85°C.
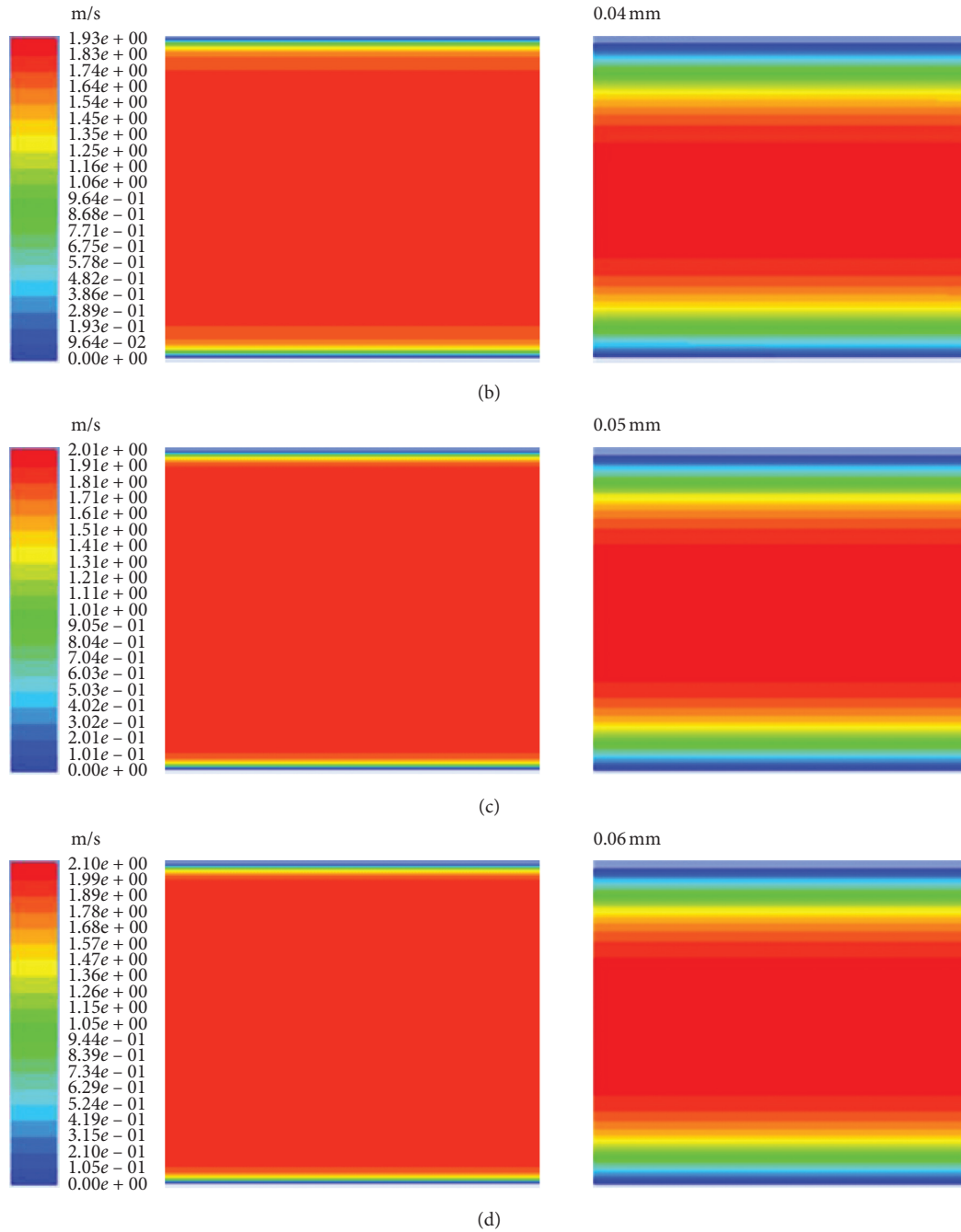

(a)

FIGURE 11: Continued.

FIGURE 11: Vectors of velocity at inlet and outlet of end clearance flow field under different clearances.

the greater the leakage flow restrained in the external gear area is.

To summarize, the direction of the centrifugal force generated by the gear rotation in the internal gear area is the same as the grease flow direction due to pressure variation. Thus, as the rotational speed increases, the leakage in the internal gear area will also gradually increase. On the other hand, the grease flow direction due to pressure variation is opposite to the centrifugal force in the leakage area of the external gear. Hence, the leakage flow will decrease as the speed increases. Considering the behavior of the flow leakage

in the internal and the external gear areas, it can be concluded that the increase of rotational speed will reduce the leakage of end clearance.

4. Leakage Model Establishment and Leakage Mechanism Analysis

Main type of internal leakage is the internal gear pump leaking at its end clearance. Due to the peculiar rheological features of grease, it is necessary to establish an adequate mathematical model of end clearance leakage to accurately
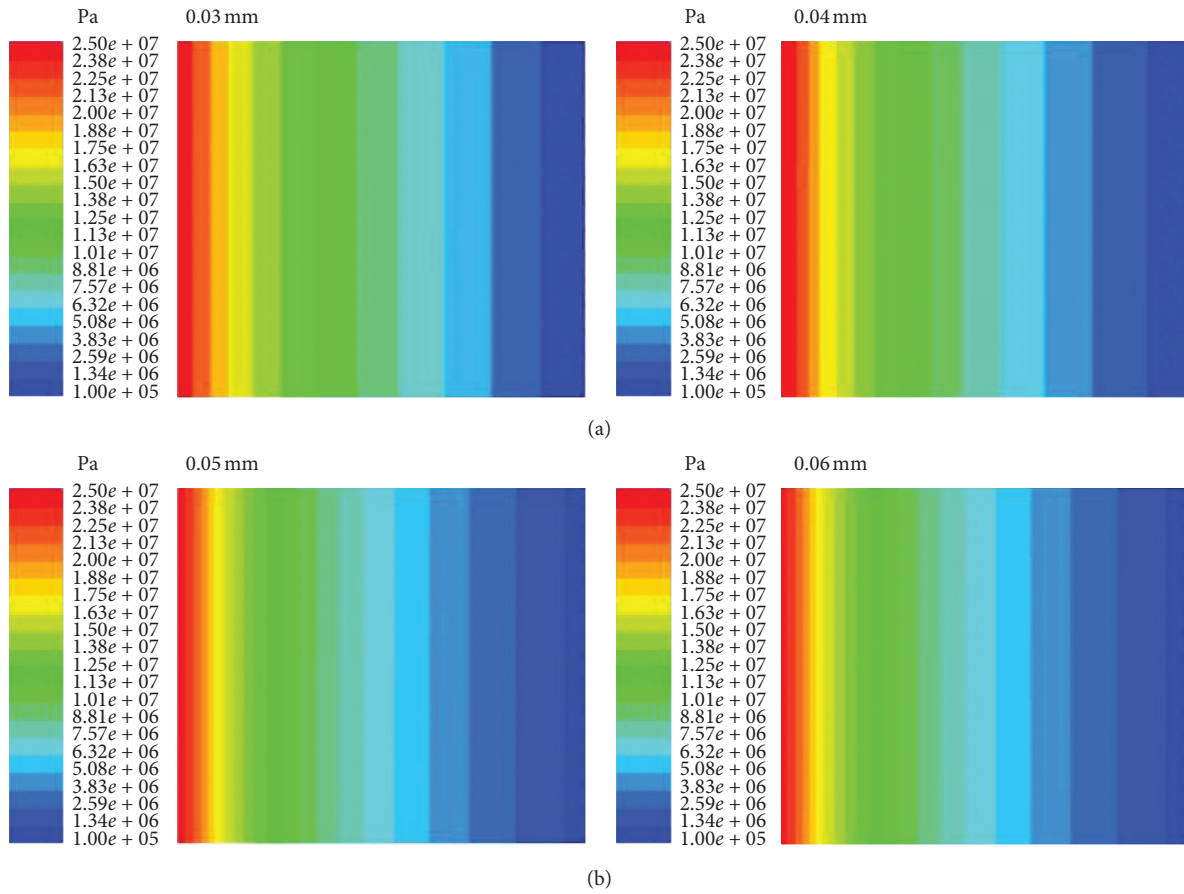
(a)

(b)

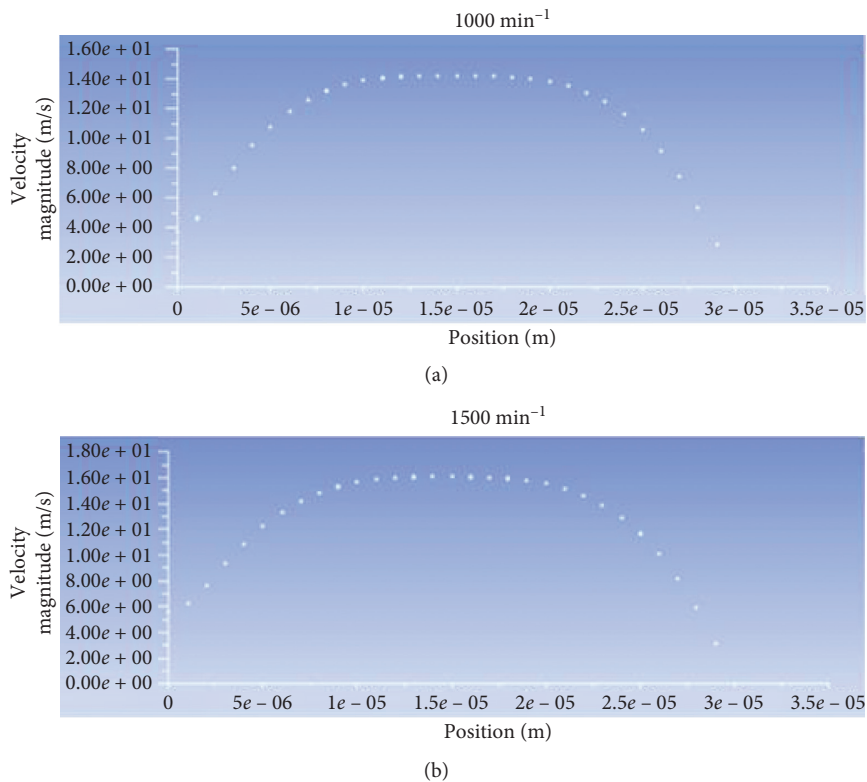FIGURE 12: Vectors of pressure at inlet and outlet of end clearance flow field under different clearances.

(a)

(b)

FIGURE 13: Continued.
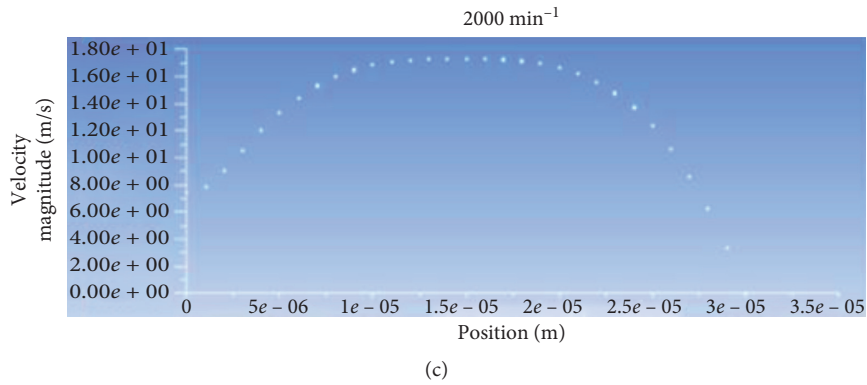
2000 min^{-1}

(c)

FIGURE 13: Speed scatter plot of the outlet of the internal gear area along the clearance direction at each speed.

(a)

(b)

(c)
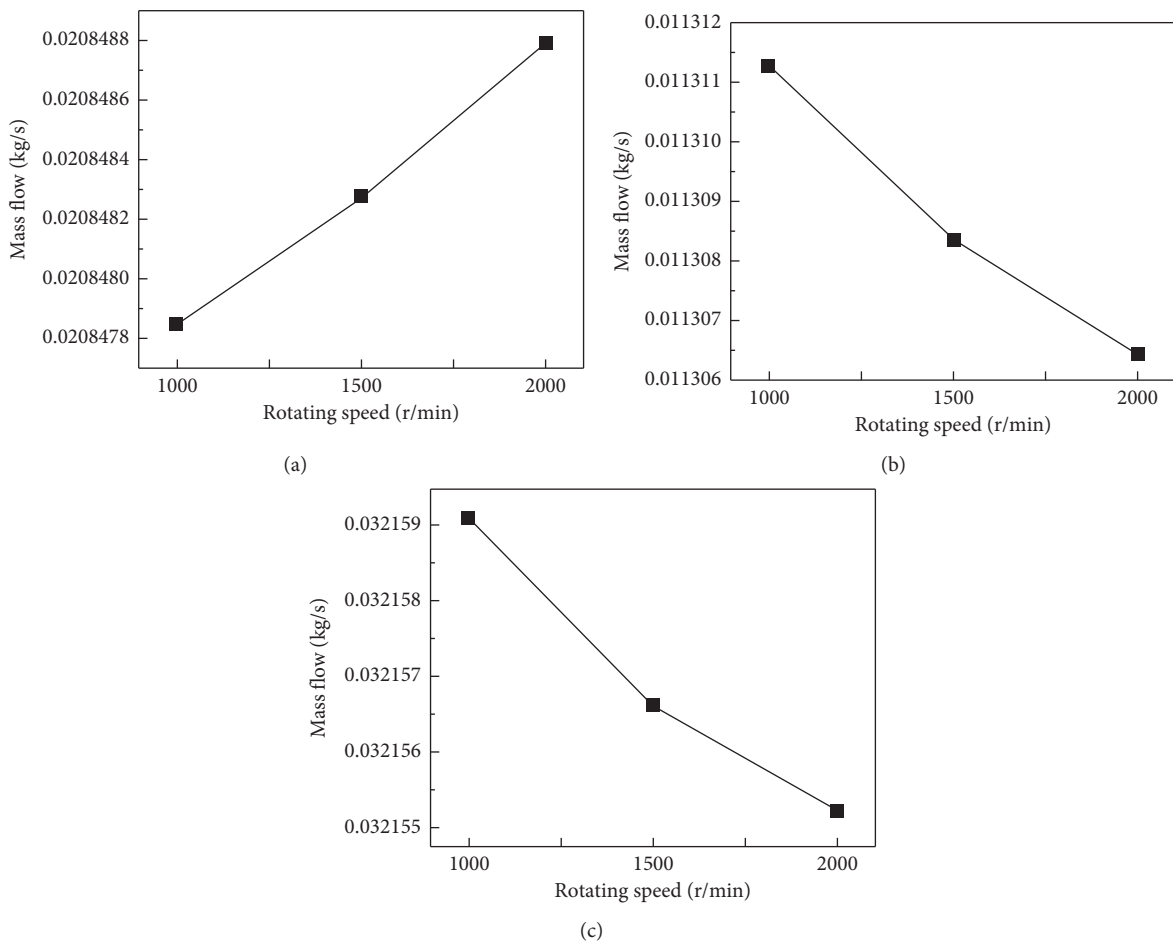
FIGURE 14: Leakage flow curve of end clearance at different speeds. (a) Leakage curve of internal gear area. (b) Leakage curve of external gear area. (c) Total leakage curve of end clearance.

explore the end clearance leakage mechanism of the internal gear grease pump.

4.1. Leakage Model Establishment.
With grease being a non-Newtonian fluid with its own flow constitutive equation, the flow of grease follows the basic equations of fluid mechanics.

Since grease is an incompressible fluid, the following leakage model can be employed:

Continuity equation:

$$\frac{\partial \rho}{\partial t} + \nabla \cdot (\rho v) = 0. \tag{2}$$

Equation of motion:

FIGURE 15: Schematic diagram of the influence of rotational speed on end clearance leakage.

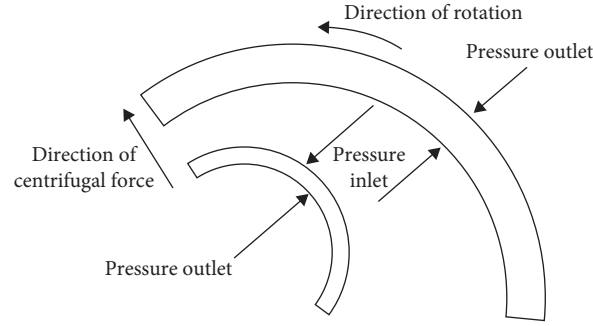$$\rho \frac{Dv}{Dt} = -\nabla \cdot p + \nabla \cdot \sigma + \rho f. \qquad (3)$$

Energy equation:

$$\rho_{cv} \frac{DT}{Dt} = -\nabla \cdot q + \sigma : \nabla v. \qquad (4)$$

According to the research content provided in Section 2, the viscosity and flow of grease are influenced by the shear rate. Figure 16 shows the relationship between the flow pattern of the grease at the plate clearance and the shear rate.

When the external force received by the grease increases and eventually exceeds the yield strength, the grease starts to flow simultaneously with the shear rate value being largest at the wall. However, in the center area, the grease still has a plug flow state, which is called a flow core. With an increase in the shear rate, the flow core eventually disappears, and the grease obtains laminar flow state between the plate clearance.

Pan et al. [21] analyzed the flow of grease and found that the Reynolds number of the conventional grease flow differs from the critical Reynolds number by two orders of magnitude. This observation contributed to the fact that the internal gear pump had a smaller end clearance during high pressure operation of the gear pump. When the working conditions were stable, the grease flow eventually turned laminar at the end clearance. Figure 17 depicts flow field model of clearance leakage, where the plate length is denoted as L, the width as b, and the clearance size as δ.

Based on the rectangular coordinate system, the basic equation of the grease flow pattern at the plate clearance is expanded and solved. Following the expansion, equations (2)–(4) can be written as follows:

Continuity equation:

$$\frac{\partial \rho}{\partial t} + \frac{\partial (\rho v_x)}{\partial x} + \frac{\partial (\rho v_y)}{\partial y} + \frac{\partial (\rho v_z)}{\partial z} = 0. \qquad (5)$$

Equation of motion:
x direction:

$$\rho \left(\frac{\partial v_x}{\partial t} + v_x \frac{\partial v_x}{\partial x} + v_y \frac{\partial v_x}{\partial y} + v_z \frac{\partial v_x}{\partial z} \right) = -\frac{\partial p}{\partial x} + \frac{\partial \tau_{yx}}{\partial y} + \frac{\partial \tau_{zx}}{\partial z} + \rho f_x. \qquad (6)$$

y direction:

FIGURE 16: Flow pattern of grease flat extrusion.
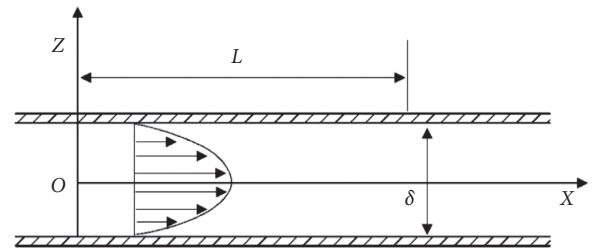
FIGURE 17: Flow field model of clearance leakage.

$$\rho \left(\frac{\partial v_y}{\partial t} + v_x \frac{\partial v_y}{\partial x} + v_y \frac{\partial v_y}{\partial y} + v_z \frac{\partial v_y}{\partial z} \right) = -\frac{\partial p}{\partial y} + \frac{\partial \tau_{xy}}{\partial y} + \frac{\partial \tau_{zy}}{\partial z} + \rho f_y. \qquad (7)$$

z direction:

$$\rho \left(\frac{\partial v_z}{\partial t} + v_x \frac{\partial v_z}{\partial x} + v_y \frac{\partial v_z}{\partial y} + v_z \frac{\partial v_z}{\partial z} \right) = -\frac{\partial p}{\partial z} + \frac{\partial \tau_{xz}}{\partial y} + \frac{\partial \tau_{yz}}{\partial z} + \rho f_z. \qquad (8)$$
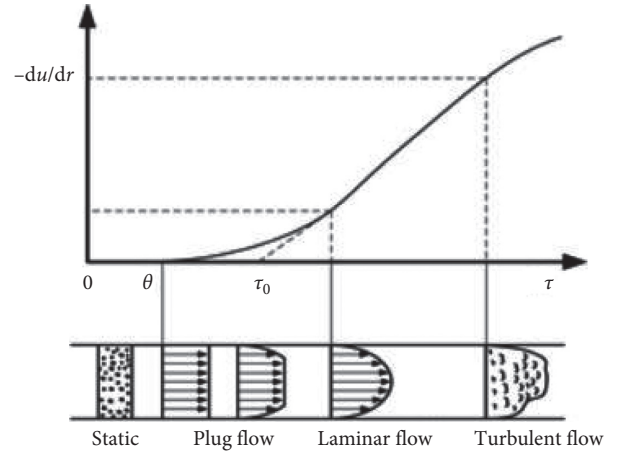
Energy equation:

$$\rho_{cv} \frac{DT}{Dt} = -\left(\frac{\partial q_x}{\partial x} + \frac{\partial q_y}{\partial y} + \frac{\partial q_z}{\partial z}\right) + \left(\tau_{xx}\frac{\partial v_x}{\partial x} + \tau_{yy}\frac{\partial v_y}{\partial y} + \tau_{zz}\frac{\partial v_z}{\partial z}\right)$$
$$+ \left(\tau_{xy}\frac{\partial v_y}{\partial x} + \tau_{xz}\frac{\partial v_z}{\partial x} + \tau_{yz}\frac{\partial v_z}{\partial y}\right). \tag{9}$$

4.2. Model Solving. Following the simplification of the equation according to the actual boundary conditions, the aforementioned equations can be written as follows:

Continuity equation:

$$\frac{\partial v_x}{\partial x} = 0. \tag{10}$$

Equation of motion:

$$\frac{\partial p}{\partial x} = \frac{\partial \tau_{zx}}{\partial z}. \tag{11}$$

H-B model:

$$\tau = \tau_0 + k\dot{\gamma}^n. \tag{12}$$

where τ is the shear stress during grease flow, τ_0 is the shear yield strength, k is the consistency coefficient, $\dot{\gamma}$ is the shear rate, and n is the grease shear thinning index.

According to the content of Chapter 2, the grease flow characteristics conform to the H-B model. Combined with the H-B model, the shear force of the grease can be obtained:

$$\tau_{zx} = \tau = \tau_0 + k(\dot{\gamma})^n = \tau_0 + k\left(\frac{\partial v_x}{\partial z}\right)^n. \tag{13}$$

Equation (13) can then be solved for the flow pattern of the grease at the plate clearance:

$$\tau_{zx} = z\frac{\partial p}{\partial x} + C_1. \tag{14}$$

When $z = 0$, v_x reaches the maximum value. $\tau_{zx} = 0$ is inserted into equation (12), while equation (14) is substituted into (12).

$$\tau_0 + k\left(\frac{\partial v_x}{\partial z}\right)^n = z\frac{\partial p}{\partial x}. \tag{15}$$

By solving equation (15), the following expression is obtained:

$$v_x = \frac{n}{n+1}\left(\frac{z}{k}\frac{\partial p}{\partial x} - \frac{\tau_0}{k}\right)^{n+1/n} \cdot k\left(\frac{\partial p}{\partial x}\right)^{-1} + C_2. \tag{16}$$

By substituting $z = \pm\delta/2$ and $v_x = 0$ into equation (16), C_2 can be obtained:

$$C_2 = -\frac{n}{n+1}\left(\pm\frac{\delta}{2k}\frac{\partial p}{\partial x} - \frac{\tau_0}{k}\right)^{n+1/n} \cdot k\left(\frac{\partial p}{\partial x}\right)^{-1}. \tag{17}$$

For $-\delta/2 \le z \le 0$ and $0 < z \le \delta/2$, v_x is equal to

$$v_x = \frac{n}{n+1}\left(\frac{1}{k}\right)^{1/n}\left(\frac{\partial p}{\partial x}\right)^{-1}\left[\left(z\frac{\partial p}{\partial x} - \tau_0\right)^{n+1/n} - \left(-\frac{\delta}{2}\frac{\partial p}{\partial x} - \tau_0\right)^{n+1/n}\right], \quad -\frac{\delta}{2} \le z \le 0, \tag{18}$$

$$v_x = \frac{n}{n+1}\left(\frac{1}{k}\right)^{1/n}\left(\frac{\partial p}{\partial x}\right)^{-1}\left[\left(z\frac{\partial p}{\partial x} - \tau_0\right)^{n+1/n} - \left(\frac{\delta}{2}\frac{\partial p}{\partial x} - \tau_0\right)^{n+1/n}\right], \quad 0 < z \le \frac{\delta}{2}. \tag{19}$$

By deriving for z in equations (18) and (19), the shear rate equation becomes

$$\frac{dv_x}{dz} = \left(\frac{1}{k}\right)^{1/n}\left(z\frac{\partial p}{\partial x} - \tau_0\right)^{1/n}. \tag{20}$$

Finally, by combining equation (20) and the H-B model, the distribution of the shear stress is obtained:

$$\tau_{zx} = \tau = \tau_0 + k(\dot{\gamma})^n = \tau_0 + k\left[\left(\frac{1}{k}\right)^{1/n}\left(z\frac{\partial p}{\partial x} - \tau_0\right)^{1/n}\right]^n$$
$$= z\frac{\partial p}{\partial x}, \quad -\frac{\delta}{2} < z \le \frac{\delta}{2}. \tag{21}$$

From equation (21), it can be noticed that the shear stress varies linearly with z value, and the shear stress is related to the pressure gradient $\partial p/\partial x$ [22], which indicates that the stress distribution of the grease at the clearance is related to the working pressure of the pump. When the working pressure of the pump increases, the shear stress and the power loss due to viscous friction increase accordingly.

5. End Clearance Optimization

The end clearance leakage of the internal gear grease pump rises with an increase in clearance value. On the other hand, if the clearance is too small, it will cause wearing of the floating side plate and the end face of the gear. This, in turn, will increase the clearance, as well as the leakage, while simultaneously reducing the service life of the pump. When optimizing the design of the end clearance, two factors are usually considered. One is the power loss caused by the flow leakage, while the other one is the friction caused power loss.

5.1. Power Loss of Flow Leakage. Due to the high internal pressure of the pump, the grease will leak towards the low-pressure zone through the end clearance, causing the energy and power losses of the pump. According to Wang [14] research, the trapped oil volume changed on parabolic rule with the increase of tooth turning angle. The angle of the trapped oil reduced on linear relationship with the increase of spiral angle. The power loss caused by the flow leakage can be expressed by

$$q = \frac{\pi \delta^3 \Delta p}{6\mu \ln(r_x/r_y)} \cdot \frac{\varphi}{2\pi}, \tag{22}$$

where μ is the fluid viscosity, r_x and r_y are the internal and external gear radius parameters, respectively, δ is the value of the end clearance, and Δp is the pressure difference due to leakage between the inlet and outlet. φ is the envelope angle of gear leakage area. By substituting the parameters of the internal and the external gear leakage, total leakage can be obtained:

$$p_q = q\Delta p = \frac{\delta^3 \Delta p^2}{6} \cdot \frac{\dot{\gamma}}{\tau_0 + k\dot{\gamma}^n} \cdot \left[\frac{\varphi_1}{\ln(r_2/r_1)} + \frac{\varphi_2}{\ln(r_4/r_3)} \right], \tag{23}$$

where q is the end clearance leakage flow, r_1 is the root circle radius of the internal gear, r_2 is the external circle radius of the internal gear, r_3 is the root circle radius of the external gear, r_4 is the radius of the gear shaft, and r_5 is the addendum circle radius of the external gear, φ_1 is the envelope angle of internal gear leakage area, and φ_2 is the envelope angle of external gear leakage area.

5.2. Power Loss of Internal Friction. The power loss area of internal friction is divided into the leakage area of the internal gear and the leakage area of the external gear. The power loss area of internal friction of the external gear includes the area from the root circle of the external gear to the gear shaft, as well as the root circle to the addendum circle. The power loss area of internal friction of the internal gear includes the root circle of the internal gear to the outer circle area of the gear shaft's internal gear and the area from the root circle to the addendum circle.

Internal fluid friction force at the end clearance can be calculated by taking the external gear as an example:

$$dF = \tau_0 + k\dot{\gamma}^n \, dA, \tag{24}$$

where F is the internal friction force of fluid at end clearance, and A is a small area from the root circle to the gear shaft. The shape of the floating side plate can be regarded as a semicircular one. A small area from the root circle to the gear shaft is taken:

$$dA = \pi r \, dr, \tag{25}$$

where r is the radius of the internal or the external gear. Assuming that the angular velocity of the gear is ω, the linear velocity of the small area is

$$v = \omega r. \tag{26}$$

Therefore, the power loss area of internal friction between the tooth circle and the gear shaft is

$$P_1 = \int_{r_4}^{r_3} dP + = \int_{r_4}^{r_3} \omega r \, dF$$
$$= \frac{1}{3}\tau_0 \pi \omega (r_3^3 - r_4^3) \left(\frac{k\pi \omega^{n+1} \delta^{-n}}{n+3} \right)(r_3^{n+3} - r_4^{n+3}). \tag{27}$$

The shape of the floating side plate is approximately semicircular. Thus, only half of the total area of the internal and external gears contains friction clearance with the floating side plate.

$$dA = \frac{\pi r \, dr}{2}. \tag{28}$$

The friction power loss from the root circle to the addendum circle area can be calculated as

$$P_2 = \int_{r_3}^{r_5} dP_f + = \int_{r_3}^{r_5} \omega r \, dF_f$$
$$= \frac{1}{6}\tau_0 \pi \omega (r_5^3 - r_3^3) \left(\frac{k\pi \omega^{n+1} \delta^{-n}}{2n+6} \right)(r_5^{n+3} - r_3^{n+3}). \tag{29}$$

In a similar manner, the friction power losses from the root circle to the outer circle of the internal gear, P_3, as well as the friction power loss from the root circle to the addendum circle of the internal gear, P_4, are

$$P_3 = \frac{1}{3}\tau_0 \omega \pi (r_2^3 - r_1^3) + \left(\frac{k\pi \omega^{n+1} \delta^{-n}}{n+3} \right)(r_2^{n+3} - r_1^{n+3}), \tag{30}$$

$$P_4 = \frac{1}{6}\tau_0 \pi \omega (r_1^3 - r_6^3) + \left(\frac{k\pi \omega^{n+1} \delta^{-n}}{2n+6} \right)(r_1^{n+3} - r_6^{n+3}), \tag{31}$$

where r_6 is the addendum circle radius of the internal gear.

In summary, the total friction power losses at the end clearance of the internal gear grease pump can be obtained as

$$P_f = 2(P_1 + P_2 + P_3 + P_4). \tag{32}$$

5.3. Mathematical Model Establishment. The optimal end clearance value of the internal gear grease pump mainly considers the flow leakage and friction induced power losses. The objective function is the minimum end clearance leakage total power loss. The mathematical model of the optimal end clearance is then

$$F(X) = P = \min(P_q + P_f), \tag{33}$$

where P_q is the power loss caused by the flow leakage and P_f is the power loss caused by friction. The constraint conditions are

$$\begin{cases} 25^\circ C \leq T \leq 85^\circ C, \\ \delta_{min} \leq \delta \leq \delta_{max}, \\ 600 \, \text{r/min} \leq n \leq 2000 \, \text{r/min}, \end{cases} \tag{34}$$

where T is the working temperature, δ is the end clearance, and n is the rotational speed of the pump.

Substitute the data in Table 4 into equation (33), and the optimal clearance is calculated as $\delta* = 0.0000124$ m $= 0.0124$ mm.

TABLE 4: Calculation parameters of power loss of end clearance.

Parameter	Unit	Value
Yield strength, τ_0	Pa	283
Consistency coefficient, k	Pa·S^n	43.25
Shear thinning index, n	1	0.48
Root circle radius of internal gear, r_1	mm	30.45
Outer circle radius of internal gear, r_2	mm	36
Addendum circle radius of internal gear, r_6	mm	24.66
Root circle radius of external gear, r_3	mm	15.01
Gear shaft radius, r_4	mm	12.5
Addendum circle radius of external gear, r_5	mm	20.1
Leakage envelope angle of internal gear, φ_1	rad	0.732π
Leakage envelope angle of external gear, φ_2	rad	0.88π
Variation in pressure, Δp	Pa	2.49×10^7
Pressure gradient $\partial p/\partial x$	Pa/m	4.49×10^9

6. Conclusions

In this paper, numerical and theoretical investigations have been conducted to study the rheological features of NLGI 1 lithium-based lubricating grease. Fluent software was employed to simulate the model flow field and explore the effects of temperature, end clearance size, and rotational speed on the end clearance leakage. Based on the rheological features of the grease, parameters and laws influencing the end clearance leakage of the internal gear grease pump were explored. The following conclusions are made:

(1) The relationship curve between the shear stress and the shear rate of NLGI 1 lithium-based lubricating grease conforms to the characteristics of the H-B model curve, while its rheological features can be utilized as data parameters for numerical simulations.

(2) The grease will flow only when the applied external force is greater than its structural strength. With an increase in temperature, the entangled structure of the grease is transformed, which has a beneficial effect on grease fluidity.

(3) The entangled network structure of grease has a dynamic evolution process. When the shear stress stops or the temperature decreases, its entangled structure can restore to its original shape.

(4) The end clearance leakage flow increases linearly with an increase in the pump temperature. The optimal temperature for pump operation is 65°C. When both clearance and temperature values are uniform, the end clearance leakage decreases as the rotational speed rises.

(5) It can be concluded that the grease end clearance flow pattern is laminar. End clearance grease flow is determined by its rheological features (τ_0, k, n) and the gear pump's operating parameters ($\delta, \partial p/\partial x$). The mathematical model of the optimal end clearance is established, based on which an optimal clearance of $\delta* = 0.0124$ mm is determined.

Data Availability

The data used to support the findings of this study are included within the article.

Conflicts of Interest

The authors declare that they have no conflicts of interest.

Acknowledgments

References

[1] W. Schweiger, W. Schoefmann, and A. Vacca, "Gerotor pumps for automotive drivetrain applications: a multi domain simulation approach," *SAE International Journal of Passenger Cars-Mechanical Systems*, vol. 4, no. 3, pp. 1358–1376, 2011.

[2] S. Guo, D. Chen, and X.-Q. He, "Calculation of unloading area of internal gear pump and optimization," *Mathematical Problems in Engineering*, vol. 2020, Article ID 7319871, 2020.

[3] Q.-l. Zeng, Z.-y. Sun, L.-r. Wan, Y. Yang, H.-z. Dai, and Z.-k. Yang, "Research and comparative analysis of flow field characteristics and load-independent power losses of internal and external gear pairs," *Mathematical Problems in Engineering*, vol. 2020, Article ID 8860588, 19 pages, 2020.

[4] S. YuanJing, Q. ZhiYuan, and Z. GuoChao, "Optimization design of internal gear pump based on improved particle swarm optimization," *Journal of Mechanical Strength*, vol. 41, no. 06, pp. 1378–1383, 2019.

[5] J. Zhang, S. Wang, X. Jiang, and X. Chen, "Optimization design of multi-teeth parallel internal gear pump based on genetic algorithm," *Modern Manufacturing Engineering*, vol. 04, pp. 115–118+152, 2018.

[6] K. Gu, Z. Wang, G. Li, and X. Liu, "Optimization of geometric parameters of the straight conjugate internal gear pump based on GA," *Journal of Electronic Science and Technology*, vol. 30, no. 06, pp. 39–42, 2017.

[7] C.-f. Wang and C.-x. Zhou, "Optimum design of external gear pump with matlab," *Mechanical Engineering*, vol. 07, pp. 119-120, 2011.

[8] E. C. Bingham, *Fluidity and Plasticity*, McGraw-Hill, New York, NY, USA, 1922.

[9] W. H. Herschel and R. Bulkley, "Measurement of consistency as applied to rubber-benzine solutions," *Proceedings of the American Society of Testing Materials*, vol. 26, pp. 621–633, 1926.

[10] A. V. Radulescu, "Radulescu I Rheological models for lithium and calcium greases," *Mechanika*, vol. 59, no. 3, pp. 67–70, 2006.

[11] A. Mohamed, "Rheological behavior of carbon nanotubes as an additive on lithium grease," *Journal of Nanotechnology*, vol. 2013, Article ID 279090, 1385 pages, 2013.

[12] B. J. Hamrock and D. Dowson, *Ball Bearing Lubrication*, pp. 243–252, Wiley & Sons, New York, NY, USA, 1981.

[13] S. K. Yeong, P. F. Luckham, and T. F. Tadros, "Steady flow and viscoelastic properties of lubricating grease containing various thickener concentrations," *Journal of Colloid and Interface Science*, vol. 274, no. 1, pp. 285–293, 2004.

[14] T. Wang, Z. Li, J. Li, and Q. He, "Impact of boron nitride nanoparticles on the wear property of lithium base grease," *Journal of Materials Engineering and Performance*, vol. 29, no. 8, pp. 4991–5000, 2020.

[15] J. B. Pan, Y. H. Cheng, and J. Y. Yang, "Effect of heat treatment on the lubricating properties of lithium lubricating grease," *RSC Advances*, vol. 5, no. 72, pp. 58686–58693, 2015.

[16] L. G. Westerberg, T. S. Lundström, E. Höglund, and P. M. Lugt, "Investigation of grease Flow in a rectangular channel including wall slip effects using Microparticle Image Velocimetry," *Tribology Transactions*, vol. 53, no. 4, pp. 600–609, 2010.

[17] J. B. Pan, Y. H. Chen, M. Qian, and B. Zhou, "Thermal-rheological features and variation mechanisms of lithium lubricating grease," *Chemical Industry and Engineering Progress*, vol. 37, no. 04, pp. 1509–1515, 2018.

[18] J. D. Dobrowolski, M. Gawliński, M. Paszkowski et al., "Experimental study of lubricating grease flow inside the gap of a labyrinth seal using microparticle image velocimetry," *Tribology Transactions*, vol. 61, no. 1, pp. 1–10, 2016.

[19] A. Vasishth, P. Kuchhal, and G. Anand, "Study of rheological properties of industrial lubricants," *Conference Papers in Science*, vol. 2014, Article ID 324615, 5 pages, 2014.

[20] L. Cheng-hui, D. Rui-long, X. An-huan, and Z. Hua, "Numerical simulation of internal gear pump flow field," *Chinese Hydraulics*, no. 07, pp. 107–110, 2015.

[21] J. B. Pan, Y. H. Chen, S. Cao, and J. Y. Yang, "Numerical simulation of thermal rheological effect on the flow field of lithium lubricating grease during pipeline flow," *Journal of Engineering Thermophysics*, vol. 36, no. 7, pp. 1563–1567, 2015.

[22] G.-l. Yang and M.-x. Li, "Trapped oil characteristics study on external helical involute gear pump," *Chinese Hydraulics*, no. 01, pp. 122–124, 2016.